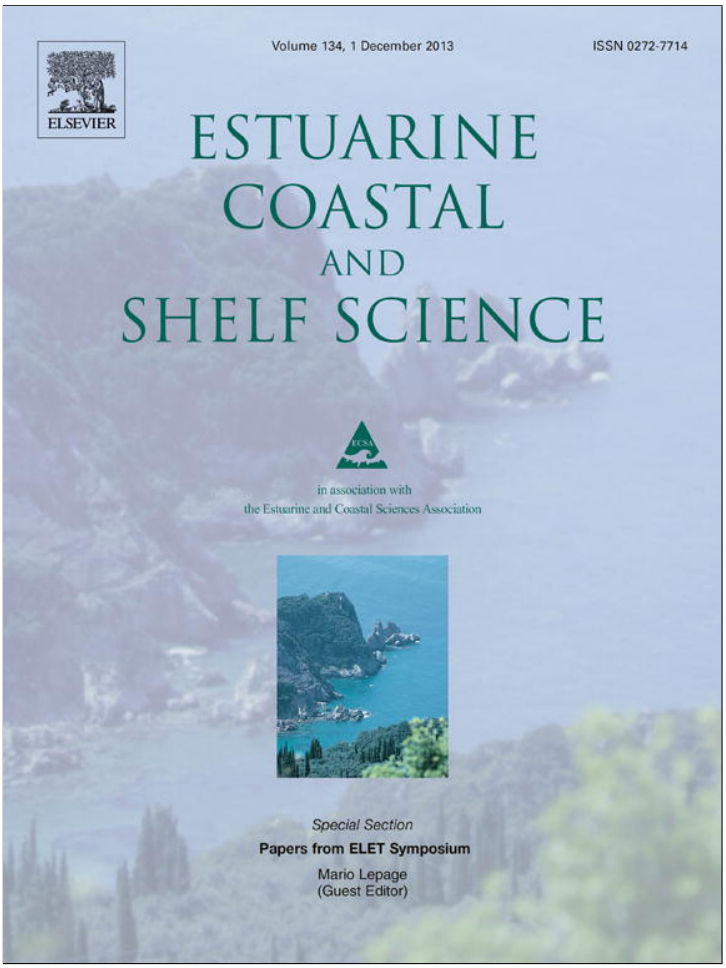

Estuarine, Coastal and Shelf Science 134 (2013) 69–79

Contents lists available at ScienceDirect

Estuarine, Coastal and Shelf Science

journal homepage: www.elsevier.com/locate/ecss

# Numerical estimation of inflow flux of floating natural macro-debris into Tokyo Bay

T. Kataoka [a, *], H. Hinata [a, 1], Y. Nihei [b, 2]

[a] Coastal Systems Division, Coastal, Marine and Disaster Prevention Department, National Institute for Land and Infrastructure Management, 3-1-1 Nagase, Yokosuka, Kanagawa 239-0826, Japan
[b] Department of Civil Engineering, Tokyo University of Science, 2641 Yamazaki, Noda, Chiba 278-8510, Japan

ARTICLE INFO

*Article history:*
Received 27 March 2013
Accepted 6 September 2013
Available online 19 September 2013

*Keywords:*
debris flow
Japan
Tokyo Bay
radar
particle motion
inversions

ABSTRACT

We numerically estimated the inflow flux of terrestrial grass, which is the main floating macro-debris, into Tokyo Bay from April 2008 to March 2009 based on a two-way particle-tracking model and an inverse method applying a Lagrange multiplier. In the estimation, we used surface current velocities derived by high-frequency ocean radar and the quantity of grass collected by clean-up vessels which are operated daily in the bay. At least 2115 $m^3$ $yr^{-1}$ of the grass flowed into the bay annually, and the contribution of a flood event to the inflow flux of grass was larger than that of the inflow flux of freshwater. We show that 39% of the annual inflow flux of grass into the bay was collected, and 61% flowed out of the bay or sank to the seabed. The numerical estimation in this study will be useful to establish a system for predicting patches of floating macro-debris in the bay, and to evaluate the effects of river development or clean-up along river banks and flood plains in the upper reaches.



## 1. Introduction

Estimating fluxes of debris from the land into the ocean is crucial in order to take measures, and to understand the impacts on the marine environment. Most studies on marine debris have focused on contamination of the marine and coastal environment by anthropogenic debris (e.g., Moore et al., 2001; Ryan et al., 2009; Law et al., 2010). Although large quantities of natural debris flowing into the ocean from the land due to natural disasters affect human activities such as sailing and marine leisure activities in the coastal zone, few studies have focused on natural debris (e.g., Moore and Allen, 2000). In addition, natural debris flowing into the ocean would contribute to the marine ecosystem, such as the oceanic carbon cycle, because terrestrial organic matter like natural debris represents a substantial source of terrestrial dissolved and particulate organic carbon (Hedges et al., 1997).

Tokyo Bay is located on the southeast coast of the main island of Japan (Fig. 1(a)). The bay plays a key role for industry in Japan, with some 600 freighters passing through the bay mouth each day, and the bay is heavily eutrophicated due to terrestrial loads (Furukawa and Okada, 2006). To ensure safety for users of the bay and to protect its marine environment, the five port administrators of Tokyo, Kawasaki, Yokohama, Chiba, Kisarazu as well as the Ministry of Land, Infrastructure, Transport and Tourism (MLIT) have been collecting both natural and anthropogenic debris drifting in the surface layer (upper 2 m) using clean-up vessels since the 1970s (Furukawa and Okada, 2006). The collected debris is classified as macro-debris (Ryan et al., 2009) because it is collected using a skipper with slit widths of 2–6 cm (Fig. 2(a)). To identify the effect of the clean-ups, we need to assess, for instance, the ratio of the annual amount of collected debris to the annual inflow.

A common approach to quantify the inflow flux is to sample debris by various filtering systems or customized nets at suspected sources for fixed periods (e.g. Durrum, 1997; Armitage and Rooseboom, 2000; Nihei et al., 2010), and then to calculate a loading rate of the debris per unit catchment area per unit time, or per unit volume of river discharge per unit time. Generally, the loading rate from a particular source shows a time dependency and includes a history effect, such as “first flush” (Armitage and Rooseboom, 2000). The loading rate also depends on the land use pattern of the catchment area, such as urban area or forest area. Thus, long-term sampling at multiple sources is required in order to estimate the inflow flux by using the loading rates calculated from direct debris sampling.

* Corresponding author.
*E-mail addresses:* kataoka-t852a@ysk.nilim.go.jp (T. Kataoka), hinata-h92y2@ysk.nilim.go.jp (H. Hinata), nihei@rs.noda.tus.ac.jp (Y. Nihei).
[1] Tel.: +81 46 844 5025; fax: +81 46 844 1145.
[2] Tel.: +81 4 7124 1501x4031; fax: +81 4 7123 9766.

0272-7714/$ – see front matter © 2013 Elsevier Ltd. All rights reserved.
http://dx.doi.org/10.1016/j.ecss.2013.09.005

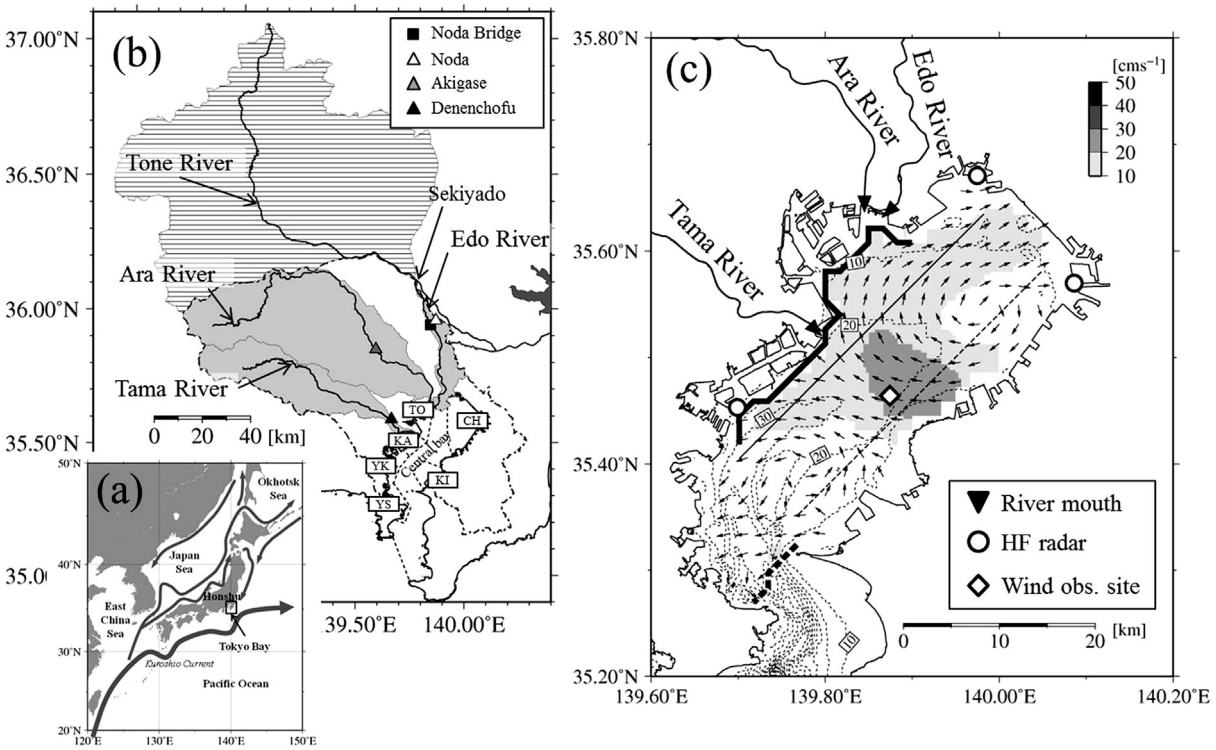


**Fig. 1.** (a) Map of Japan showing Tokyo Bay and ocean currents. (b) The catchment area of Tokyo Bay (area enclosed by thick chain line), the three large rivers flowing into the bay (gray area), and the Tone River above Sekiyado (lateral line area). Squares and triangles show sampling sites of floating macro-debris by Nihei et al. (2010) and observation sites of river level by the MLIT, respectively. The broken line shows the boundaries between port areas (Tokyo (TO), Kawasaki (KA), Yokohama (YK), Yokosuka (YS), Chiba (CH), Kisarazu (Ki)) and the central bay. (c) Bathymetric map of Tokyo Bay showing also the residual current field on 31 July 2008 measured by HF radar. The solid thin line and broken thin line in the bay show the western and eastern lines, respectively (see Fig. 8). The solid bold line and broken bold line show suspected sources of floating macro-debris and bay mouth, respectively.

Here, we numerically estimate the fluxes of grass, which was the main type of floating macro-debris (see Section 2.1), into Tokyo Bay from three large rivers (Edo River, Ara River and Tama River; Fig. 1(c)) for fiscal 2008 (from April 2008 to March 2009; F2008) based on a two-way particle-tracking model (two-way PTM) developed by Isobe et al. (2009) and an "inverse method using a Lagrange multiplier" (IMLM) developed by Kako et al. (2010) using data on the grass collected in the bay by the MLIT (see Section 2.1) and high-frequency (HF) ocean surface radar-derived surface current velocities (see Section 2.2). This numerical estimation allows us to identify the sources and to estimate the inflow fluxes without sampling debris at multiple sources. As the first step to understand the inflow flux of macro-debris in Tokyo Bay, here we estimate the order of magnitude of the inflow flux of grass flowing into the bay.

## 2. Data and method

### 2.1. Collection data of grass in Tokyo Bay

The MLIT collects macro-debris in central Tokyo Bay (Fig. 1(b)) during the daytime (9:00–16:00) on weekdays. Most of the debris collected in F2008 was natural debris (Fig. 2(d)); only 4% was anthropogenic debris such as plastic bags and sheets, bottles, cans, styrofoam products, and electronic products. The daily volume of the debris is measured by placing it in containers with a scale at the home port. In F2008, the maximum and the average of the daily collected volume were 28.7 $m^3$ and 4.6 $m^3$, respectively. We selected grass, which accounted for 29% (Fig. 2(d)), to facilitate the particle-tracking experiments for the numerical estimation because the advection process of grass is not strongly affected by the wind. Since the collected grass contains voids, we conducted a laboratory experiment to estimate the net ratio (see Appendix A) and hence compute the net volume of grass. The net volume was computed by multiplying the net ratio (0.3661) by the collected volume (Table 1).

The collection points and the volume of grass collected at each point are not recorded. The speed of the vessel is reduced to 4 knots (2.06 m $s^{-1}$) or less during collection (Kataoka and Hinata, 2012). Therefore, we identified the grass collection points by calculating the vessel speed based on the track recorded every 4 s by the global positioning system (GPS). Typically, a vessel goes back and forth inside a patch of debris until no debris can be found during the collection and its track also forms a patch (hereafter, "collection patch"); the average position of the vessel track is taken as the collection point. The collection patch is approximated as an ellipse, and its average area in F2008 was approximately 0.765 $km^2$ (Kataoka and Hinata, 2012). The volume collected at each collection point is calculated by allocating the daily collected volume of grass to each point in proportion to the duration of each collection. Tracks were not recorded on some of the operation dates in F2008. In the IMLM, only the net collected volume on the track recording date (value within parentheses in Table 1) was used.

The total volume of debris that was collected by the port administrators was recorded daily, but the collected volume of grass and the tracks of the collection vessels are not available. We assumed that the composition and the net ratio of grass collected by the administrators are the same as those of grass collected by the MLIT. The net volume of grass was calculated by multiplying the volume collected by the administrators by the collection ratio of grass (29%) and the net ratio (0.3661) (Table 1).

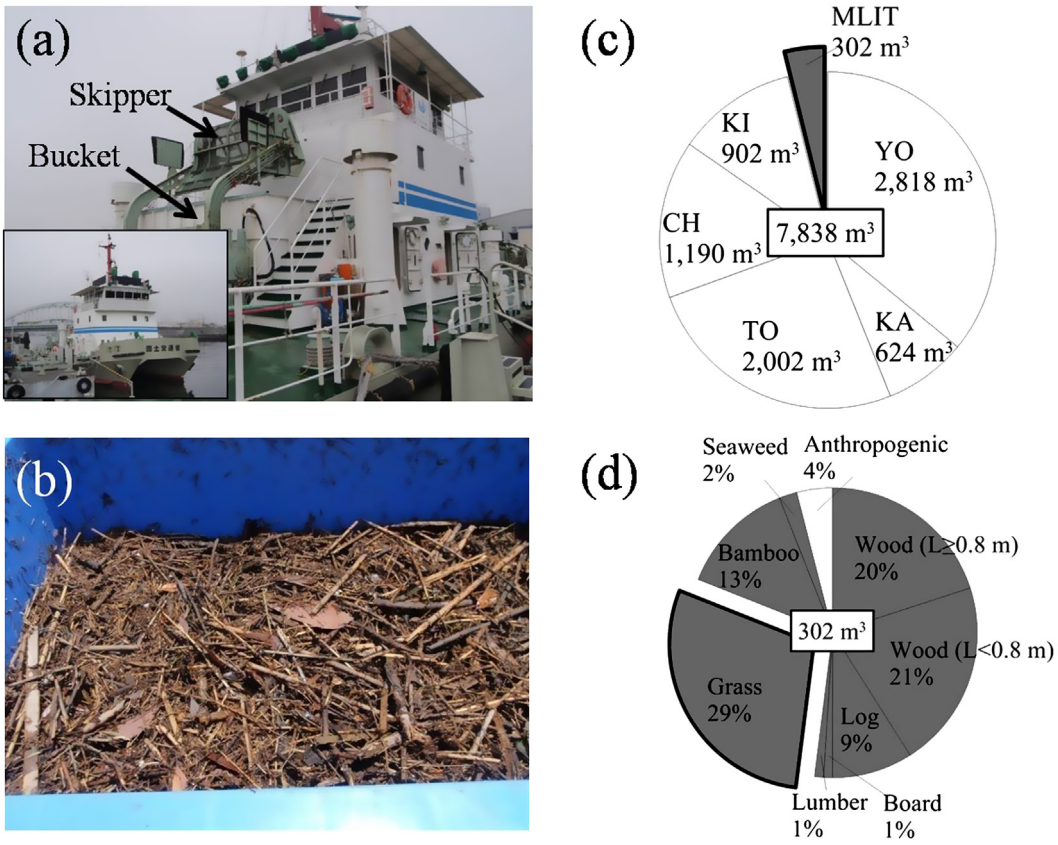


**Fig. 2.** Photographs of the MLIT clean-up vessel (a) and grass collected in the bay (b). (c) Quantity of floating macro-debris collected by the MLIT and the port administrators in the bay in F2008. (d) Composition of floating macro-debris collected by the MLIT (natural debris is shaded in gray) in F2008.

### 2.2. HF radar-derived surface current velocities

We use the HF radar-derived surface current velocity data set for F2008 produced by Kataoka and Hinata (2012). The specifications of the HF radar system (Nagano Japan Radiowave Co., Ltd.) are shown in Table 2. The estimated error of the radar system based on a comparison between the velocities measured by the HF radar system and those measured by acoustic Doppler current profilers (ADCP) is $\pm 6$ cm s$^{-1}$ for both the EW and NS components (Yanagi et al., 2003).

Dividing the bay into 347 grid points at 1.5-km intervals, the surface velocity vectors at 250 of the 347 grid points can be obtained from two or three HF radar-derived radial velocities. At the other grid points where one or no radial velocity was measured, the velocity vectors were estimated by extrapolating from the observed velocity vectors around the grid points using the inverse distance weighted method with a $1/d^2$ type of weight function and the velocity components at the grid points on the land being zero (Kataoka and Hinata, 2012). The HF radar failed to obtain surface velocities for 1 month from 28 January 2009 to 28 February 2009 because of a malfunction of the HF radar system.

### 2.3. Source identification and inflow flux estimation

Our numerical model consists of the two-way PTM to identify the sources of grass (Isobe et al., 2009) and the IMLM to estimate inflow fluxes of grass per unit time from each source identified by the two-way PTM (Kako et al., 2010). To identify sources and to estimate the inflow fluxes, Kako et al. (2010) used accumulation rates obtained by a bimonthly beach survey and modeled surface current velocities on the East China Sea continental shelf. We used the volume of grass collected by the MLIT and the HF radar-derived surface current velocities instead. The applicability of these methods to Tokyo Bay has already been confirmed by Kataoka and Hinata (2012), who found that the error of identifying sources by the two-way PTM is within 10 km, and the error of estimating the inflow flux is 0.9–1.6 times the true flux.

#### 2.3.1. Two-way PTM

Two-way PTM experiments were carried out to identify sources of grass by combining a “backward-in-time” PTM with a “forward-in-time” PTM. The details of the PTM are given in Appendix B. First, backward-in-time PTM experiments were carried out to determine the source candidates of grass. In these experiments, 5000 particles placed at the collection points at the collection time were tracked by the HF radar-derived surface currents with directions reversed in sign for both horizontal current components in conjunction with random-walk processes. “Random-walk” means the trajectories of successive random steps computed by the last term of Eq. (B.1) in Appendix B. These particles were tracked until they reached the 1.5-km grid boxes of the western boundary covered by HF radar near the mouths of the three large rivers and/or outfalls (bold line in Fig. 1(c)). To determine the source candidates in the backward-in-time PTM experiments, the 1.5-km grid boxes were divided into nine boxes of 500 m in size, and the 500-m boxes were considered as source candidates. Multiple source candidates in a 1.5-km grid box were replaced with the candidate having the most particles. If the particles reached boundaries other than the bay mouth (bold broken line in Fig. 1(c)) and the western boundary (bold line in Fig. 1(c)), we performed the re-drifting operation (see

**Table 1**
The monthly freshwater flux and the monthly collection of floating macro-debris by the MLIT and the port administrators.

| | 2008 | | | | | | | | | 2009 | | | Summation |
|---|---|---|---|---|---|---|---|---|---|---|---|---|---|
| | Apr | May | Jun | Jul | Aug | Sep | Oct | Nov | Dec | Jan | Feb | Mar | |
| Freshwater flux of three rivers ($\times 10^9$ m$^3$) | 0.780 | 0.682 | 0.871 | 0.530 | 1.042 | 0.951 | 0.513 | 0.237 | 0.247 | 0.341 | 0.280 | 0.358 | 6.832 |
| *Collection by the MLIT* | | | | | | | | | | | | | |
| All debris | | | | | | | | | | | | | |
| Number of operation days[a] | 18 (16) | 19 (12) | 20 (17) | 20 (16) | 10 (8) | 18 (15) | 20 (15) | 17 (9) | 18 (15) | 18 (16) | 4 (4) | 4 (1) | 186 (144) |
| Collected volume (m$^3$)[b] | 40.46 (40.01) | 42.51 (16.03) | 17.82 (14.31) | 7.99 (6.69) | 37.74 (5.59) | 67.40 (62.41) | 38.28 (28.73) | 27.01 (20.33) | 8.03 (6.87) | 11.47 (8.68) | 1.71 (1.71) | 1.22 (0.42) | 301.64 (211.78) |
| Grass | | | | | | | | | | | | | |
| Number of operation days[a] | 12 (10) | 16 (11) | 10 (8) | 3 (3) | 9 (7) | 14 (12) | 11 (7) | 10 (5) | 0 (0) | 1 (1) | 1 (1) | 0 (0) | 87 (65) |
| Collected volume (m$^3$)[b] | 9.84 (9.60) | 15.45 (5.98) | 3.86 (2.49) | 0.37 (0.37) | 16.32 (1.37) | 19.32 (18.32) | 18.94 (14.95) | 3.74 (2.74) | 0.00 (0.00) | 0.12 (0.12) | 0.25 (0.25) | 0.00 (0.00) | 88.21 (56.19) |
| Net collected volume (m$^3$)[b] | 3.60 (3.51) | 5.66 (2.19) | 1.41 (0.91) | 0.14 (0.14) | 5.97 (0.50) | 7.07 (6.71) | 6.93 (5.47) | 1.37 (1.00) | 0.00 (0.00) | 0.04 (0.04) | 0.09 (0.09) | 0.00 (0.00) | 32.28 (20.56) |
| Average daily collected volume (m$^3$ d$^{-1}$)[c] | 0.30 | 0.35 | 0.14 | 0.05 | 0.66 | 0.51 | 0.63 | 0.14 | 0.00 | 0.04 | 0.09 | 0.00 | |
| *Collection by the port administrators* | | | | | | | | | | | | | |
| All debris | | | | | | | | | | | | | |
| Collected volume (m$^3$) | 681.34 | 850.71 | 549.14 | 690.00 | 745.21 | 1490.12 | 529.57 | 321.13 | 353.88 | 421.31 | 486.18 | 416.49 | 7535.08 |
| Grass | | | | | | | | | | | | | |
| Net collected volume (m$^3$) | 72.34 | 90.32 | 58.30 | 73.26 | 79.12 | 158.20 | 56.22 | 34.09 | 37.57 | 44.73 | 51.62 | 44.22 | 799.99 |

[a] Value within parentheses means monthly number of days the tracks of the MLIT clean-up vessel were recorded.
[b] Value within parentheses means monthly volume of debris that was collected on the days the tracks of the vessel were recorded.
[c] Average daily collected volume was calculated by dividing the net collected volume by the number of operation days.

Appendix B). We terminated the backward-in-time PTM experiments at the time step when particles reached a grid box of the bay mouth (bold broken line in Fig. 1(c)) or the corresponding monthly residence time of the surface water masses (see Appendix B).

In general, source identification using only backward-in-time PTM is unreliable because the motion of an object includes irreversible random-walk processes. Therefore, forward-in-time PTM experiments were carried out to examine whether each source candidate was statistically significant or not. In the experiments, 5000 particles were released from each source candidate identified in the foregoing backward-in-time PTM experiments, and were carried by the HF radar-derived surface currents. Also, in the forward-in-time PTM, the particles that reached the boundaries except the bay mouth continued to be tracked by the re-drifting operation, and the tracking was terminated when they reached the bay mouth. At each collection time, the particle distribution was approximated as an ellipse whose major axis length represented twice the standard deviation of the distances between particle positions and their averaged one. If the corresponding collection point was located within the ellipse, the source candidate from which these particles were released was considered to be significant at the 95% confidence level.

### 2.3.2. IMLM

The inflow fluxes of grass at each source detected in the above two-way PTM are computed using the IMLM. The relationship between the volume ($z$: a constant in each collection) which was collected by the MLIT at each collection point and inflow flux (**f**; a row vector) at various sources is given by:

$$\left(f_1^{M-l}, f_2^{M-l}, f_3^{M-l}, \ldots, f_{N-1}^{M}, f_N^{M}\right) \begin{pmatrix} g_1 \\ g_2 \\ g_3 \\ \vdots \\ g_{N\times(l+1)} \end{pmatrix} = z, \qquad (1)$$

where the subscripts represent sources ($N$: the total number), the superscripts denote the hour in which the grass flows into the bay from each source, and $M$ is the time when the MLIT collected grass corresponding to $z$, and $l$ is determined by the monthly residence time (see Appendix B). Thus, the collected volume $z$ is derived from the inflows up to $l$ hours before. The column vector **g** denotes the weights of inflows from each source at each time in determining $z$, and depends on the contribution of surface current to the behavior of grass in Tokyo Bay. The weight vector **g** can be determined by forward-in-time PTM in conjunction with a random-walk process (i.e. the last term of Eq. (B.1)) in which the particles are released from each source at each time from $M$ to $l$, and according to the number of particles that reach the collection patch (see Section 2.1). The inflow flux **f** is calculated by solving the above equation using a Lagrange multiplier. For a more thorough explanation of the determination of vector **g** and the solution of the inverse problem for the above equation, refer to Kako et al. (2010).

### 2.4. River discharge at river mouth

In Tokyo Bay, rainwater falling in the catchment area of the bay mainly flows in the three large rivers: the total catchment area (6571 km$^2$) of these rivers (Edo River, 2391 km$^2$; Ara River, 2940 km$^2$; Tama River, 1240 km$^2$; see Fig. 1(b) and (c)) accounts for 67% of the catchment area of Tokyo Bay (approximately 9800 km$^2$).

**Table 2**
Specifications of the HF radar system.

| | |
|---|---|
| Radar type | Frequency modulated interrupted continuous wave (FMICW) |
| Center frequency | 24.515 MHz |
| Sweep bandwidth | 100 kHz (24.465–24.565 MHz) |
| Frequency sweep interval | 0.5 s |
| Maximum transmission power | 200 W (peak) |
| Range resolution | 1.5 km |
| Velocity resolution | <4.78 cm s$^{-1}$ |

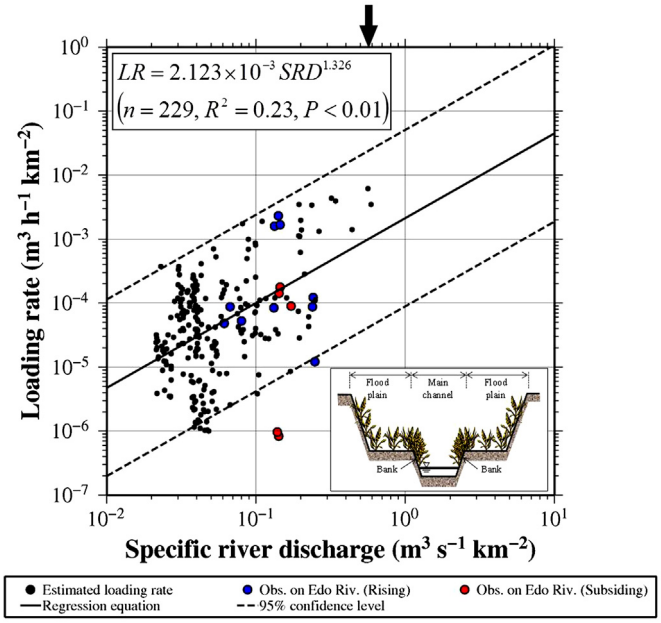


**Fig. 3.** Comparison of the relationship between the LR and the SRD obtained by this study and the net samplings of Nihei et al. (2010). The regression equation is shown in the upper left, and a typical c-section of the large rivers flowing into Tokyo Bay in lower reaches is shown in the lower right. The black arrow shows the maximum of the SRD in F2008.

Thus, most of debris would flow into Tokyo Bay through these three rivers. The catchment area of the Edo River is determined to be 2391 km$^2$ assuming that it diverges from the Tone River (Nihei et al., 2007a).

To investigate the relationship between the inflow flux of grass and the river discharge of the three large rivers, we used a data set of river discharge at a river mouth established by Nihei et al. (2007b). Briefly, this method is as follows. First, the relationship between the water level and the river discharge (i.e. rating curve) at an observation site located in the upper reaches is determined; the observation sites of the Edo River, Ara River and Tama River are respectively "Noda" located 39 km upstream, "Akigase" located 34 km upstream and "Denenchofu" located 13 km upstream (Fig. 1(b)). The river discharge at each observation site was calculated by applying the water level which was continuously observed at the sites (Water Information System by the MLIT; http://www1.river.go.jp/) to the rating curve at each site. Then, the river discharge at the river mouth was calculated by considering the inflow of other rivers and sewers, water from river branches and rainfall on the catchment of the lower reaches. The accuracy of the river discharge calculated by this method was confirmed by comparing it with the river discharge observed at the river mouth.

## 3. Results

### 3.1. Estimation of inflow fluxes of grass

Inflow fluxes of grass from sources identified by the two-way PTM every hour were numerically estimated by the IMLM in F2008. However, it was difficult to classify the inflow flux from each source (or each river) because the errors of identifying debris sources by the two-way PTM were within 10 km (Kataoka and Hinata, 2012). Therefore, hourly inflow flux was calculated from the summation of the inflow fluxes from all sources every hour.

The estimated hourly inflow fluxes were compared with the total river discharge of the three large rivers (Fig. 3). In Fig. 3,

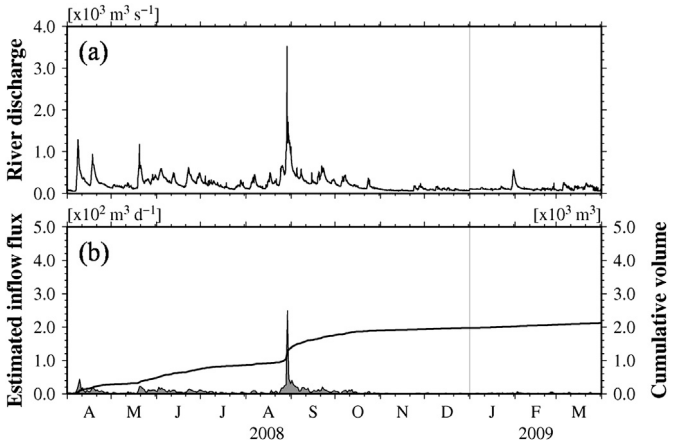


**Fig. 4.** The time series of river discharge (a) and inflow flux estimated by this study (b). The thick line in (b) is the cumulative curve of inflow flux.

"loading rate (LR)" and "specific river discharge (SRD)" are calculated by respectively dividing the hourly inflow flux and the total river discharge by the total catchment area (i.e., 6571 km$^2$).

The relationship between the flux $L$ of a substance in river water and river discharge $Q$ is frequently modeled as:

$$L = aQ^b, \tag{2}$$

where $a$ and $b$ are constants (e.g. Ebise, 1985; Takada et al., 1992). In this study, $L$ is the LR (m$^3$ h$^{-1}$ km$^{-2}$), $Q$ is the SRD (m$^3$ s$^{-1}$ km$^{-2}$), and the LR is regressed against the SRD. We found a significant relationship between the LR and the SRD at the 95% confidence level ($R^2 = 0.23$, $P < 0.01$, see Fig. 3). The coefficients $a$ and $b$ in Eq. (2) were $2.123 \times 10^{-3}$ and 1.326, respectively (black solid line in Fig. 3), and the 95% confidence interval of the coefficient $a$ ranged from $8.699 \times 10^{-5}$ to $5.181 \times 10^{-2}$ (black broken line in Fig. 3). Although the determination coefficient was low due to the large variability of the LR for the SRD of 0.02–0.3 m$^3$ s$^{-1}$ km$^{-2}$, the relationship was statistically significant. This means that the grass in the river channel was flushed out downstream by flood events.

The hourly inflow fluxes were not estimated during some periods because grass was not collected by the MLIT at certain times, namely outside of operating hours (9:00–16:00) on weekdays, weekends, holidays, and days when the vessel was maintained. In addition, surface velocities were not obtained from 28 January 2009 to 28 February 2009 (see Section 2.2). The unestimated hourly inflow fluxes were calculated by Eq. (2). In this calculation, we established a threshold value for the river discharge of each river to judge whether the river was in a flood or non-flood condition because most of the grass grows on the floodplain and the banks of the main channel, and would not flow out into Tokyo Bay in the non-flood condition because of the lower water level and the weaker current (see lower right in Fig. 3).

It is difficult to define a specific threshold value to judge the flood condition because it depends on the cross-section of the river channel. We used 0.02 m$^3$ s$^{-1}$ km$^{-2}$ as the threshold value of the SRD because hourly inflow fluxes were not estimated in the lower SRD range (Fig. 3). If the SRD calculated from the total river discharge was higher than the threshold value, the hourly inflow fluxes were calculated by multiplying the total catchment area (6571 km$^2$) by the LR, which was computed by substituting its SRD into Eq. (2).

Consequently, the daily inflow fluxes were calculated by adding the summation of the hourly inflow fluxes to the daily net volume of grass collected by the port administrators. The time series of the

daily inflow flux fluctuated as the river discharge swelled, and in particular, greatly increased on August 29 and 30 (Fig. 4(a) and (b)). The annual inflow flux was calculated by the summation of the daily inflow fluxes, and was 2115 $m^3$ $yr^{-1}$. The inflow flux (506 $m^3$ 10 $day^{-1}$) in the largest flood event (for the 10 days from 25 August to 3 September) accounted for 24% of the annual inflow flux. On the other hand, the inflow flux of freshwater for the same 10 days ($7.219 \times 10^8$ $m^3$ 10 $day^{-1}$) corresponds to 11% of the annual freshwater flux ($6.832 \times 10^9$ $m^3$ $yr^{-1}$). This indicates that the inflow flux of grass is greatly increased by flood events compared with the freshwater flux.

### 3.2. Comparison with loading rates obtained by net samplings

The low determination coefficient for the regression equation was due to the large variability of the LR for the SRD of 0.02–0.3 $m^3$ $s^{-1}$ $km^{-2}$ (Fig. 3). To confirm the variability of the LR in this range of the SRD, we compared the relationship between the LR and the SRD obtained by the IMLM with that observed by a net sampling that was conducted at the Noda Bridge across the Edo River (Nihei et al., 2010). Details of this net sampling have already been published by Nihei et al. (2010), so the observation design is explained only briefly in Appendix C. The LR and the SRD were calculated by respectively dividing the hourly inflow flux measured by the net sampling and the river discharge at each observation site, by the catchment area that was taken from the start of the Edo River to the Noda Bridge (2223.5 $km^2$). The relationship between the LR and the SRD obtained by the net sampling is shown in Fig. 3.

Consequently, the large variability of the LR for the SRD of 0.02–0.3 $m^3$ $s^{-1}$ $km^{-2}$ is reasonable because the LRs observed by the net sampling were included within the 95% confidence interval of the regression residuals, and also largely varied in the same range of the SRD (Fig. 3). We consider that the large variability of the LR was caused by the difference of the LR between the rising stage and the subsiding stage, various cross sections of river channel in the catchment area of the rivers and seasonal variations of the relationship between LR and SRD (e.g. first flush) (see Section 4.1).

### 3.3. Validation of hourly inflow fluxes by a hindcast experiment

To validate the hourly inflow fluxes, the net collected volume of grass was simulated based on the forward-in-time PTM. In the hindcast experiment, to also investigate the fate of grass on the surface in the bay, monthly residual volume (i.e. volume of grass staying in the bay) and monthly outflow (i.e. volume of grass flowed out of the bay) were computed. In this experiment, the net collected volume by the port administrators was subtracted from the hourly inflow fluxes because the MLIT cannot collect grass that has already been collected by the port administrators. The number of particles was determined by multiplying the hourly inflow fluxes by one hundred (i.e. the weight of a single particle is 0.01 $m^3$).

The sources for the hindcast experiment were the grid points along the western boundary of the HF radar coverage where the river mouths of the three large rivers and/or outfalls are located nearby (bold line in Fig. 1(c)), and the interval between the sources is 500 m. The particles were homogeneously released into the bay from each source on the hour. The particles released from each source were tracked until they were collected by the vessel or flowed out of the bay through the bay mouth (bold broken line in Fig. 1(c)). The hindcasted volume was calculated by multiplying the weight per particle (i.e., 0.01 $m^3$ per particle) by the number of particles located in the collection patch (see Section 2.1). Thus the hindcasted volume corresponds to the net volume of grass that was collected on the date on which the tracks were recorded (i.e. values within parentheses in Table 1).

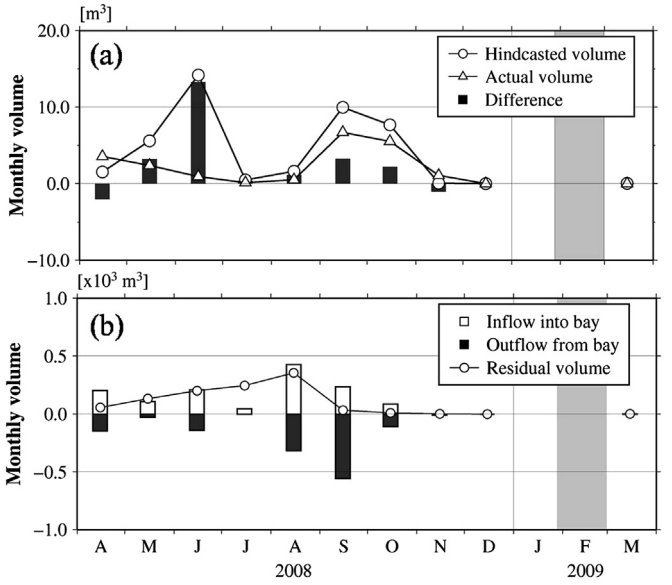


**Fig. 5.** (a) Comparison of hindcasted volume of grass collected by the MLIT with the actual volume. (b) Time series of the monthly inflow flux, the residual volume in the bay at the end of the month and the monthly outflow from the bay mouth. In January and February 2009, the hindcast experiment could not be carried out because of malfunction of the HF radar system (shaded in gray).

The monthly residual volume and the monthly outflow were calculated by multiplying the weight per particle by the number of residual particles at the end of each month in the bay and the total number of particles reaching the boundary along the bay mouth (bold broken line in Fig. 1(c)) during each month, respectively. In the experiments, if some particles reached the boundaries of HF radar coverage except the bay mouth, the re-drifting operation was performed (see Appendix B).

The monthly hindcasted volume was compared with the monthly net volume actually collected by the MLIT (Fig. 5(a)). Fig. 5(a) demonstrates that the monthly hindcasted volume indeed varies consistently with the monthly actual volume except in June 2008. The deviation in June between the monthly hindcasted volume and the monthly actual volume is 13.3 $m^3$. This overestimation is caused by the daily hindcasted volume on 2 June 2008 (9.6 $m^3$). On this date, the many particles that accumulated along the boundaries of HF radar coverage in the Yokohama port area were temporarily returned offshore by the northeastward tidal current and were collected by the vessel near the boundaries of the Yokohama port area in the hindcast experiments (star in Fig. 6(a)). The re-drifting operation performed near the boundaries would be one of the reasons for the overestimation. This paper does not further discuss the overestimation because the present PTM is unable to track drifting particles out of the HF radar coverage. Nevertheless, the monthly hindcasted volumes are reasonably consistent with the monthly actual volume (Fig. 5(a)). Fig. 5(a) indicates that the hourly inflow fluxes of grass are successfully estimated by the IMLM and the regression equation (i.e. upper left in Fig. 3).

The time series of the monthly residual volume, the monthly outflow and the monthly inflow flux from the three large rivers (i.e. the summation of the hourly inflow fluxes during each month) are shown in Fig. 5(b). The hindcast experiment revealed a seasonal variation of the monthly residual volume in the bay: the volume increased from April to August 2008, reaching 355 $m^3$ at the end of August. This corresponds to 36% of the five-month inflow (990 $m^3$) until the end of August. Conversely, residual grass (64% of the five-

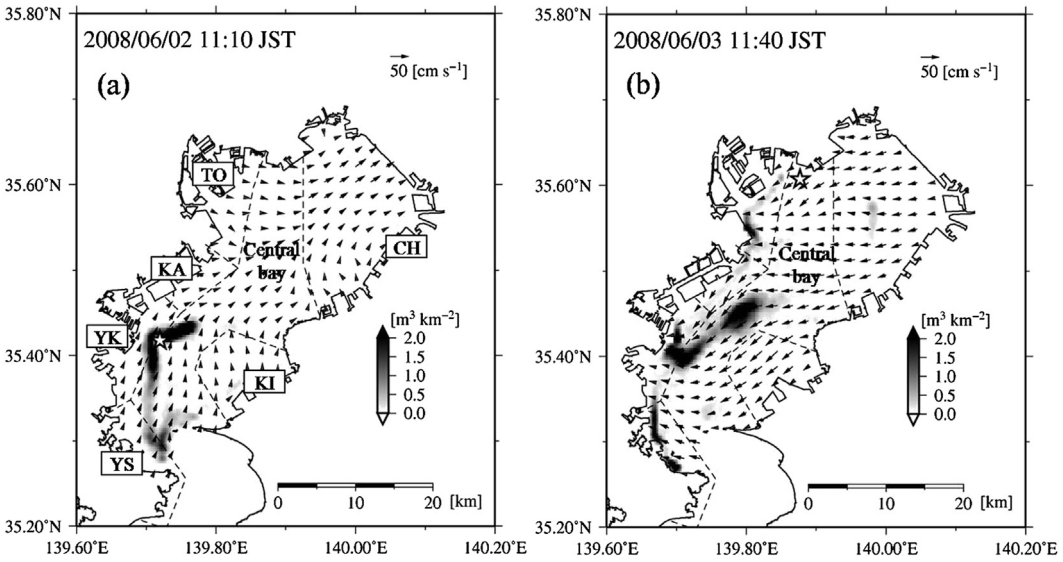


**Fig. 6.** Snapshot of the distribution of grass in the hindcast experiment and surface current pattern on 2 June (a) and 3 June (b). The gray shading and star show the quantity of grass per unit area and collection point by the MLIT, respectively. The broken lines show the boundaries between the port area and the central bay.

month inflow) flowed out of the bay until this month. It greatly decreased in September 2008 and did not increase after October 2008 because of small inflow fluxes. We consider that the seasonal variation of the residual volume reflects that of the residual current in Tokyo Bay (see Section 4.2).

### 3.4. Annual flow of grass in Tokyo Bay

We consider the annual flow of grass in Tokyo Bay as a simple, one-dimensional flow (Fig. 7). Fig. 7 shows the annual flow described based on the hindcast experiment. 39% of the annual inflow flux was collected by the port administrators and the MLIT, and the remaining grass (61% of the annual inflow flux) would flow out of the bay during one year (Fig. 7). The true inflow flux would be larger than our estimation which depends on the effort of clearance services. If the MLIT could not completely clear the debris patches due to missing grass and/or an overflow of the built-in bucket with the grass (Fig. 2(a)), the estimation is underestimated. Nevertheless, the order of magnitude of the estimation is considered to be reasonable because of the following reasons: the vessel went back and forth inside a debris patch until no grass could be found; the daily collected volume did not exceed the volume of the bucket (30 $m^3$, see Section 2.1). In addition, the average daily collected volume in each month was significantly related to the corresponding monthly freshwater flux ($R = 0.69$, $P < 0.05$, see Table 1), which indicates that larger parts of the debris patches were collected.

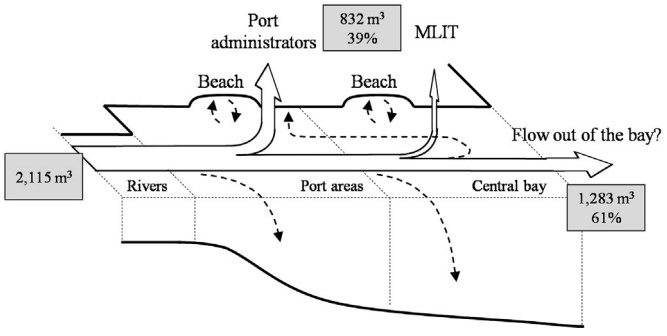


**Fig. 7.** Schematic flow diagram of grass in Tokyo Bay. The broken arrows show unknown flow in this study.

On the other hand, in reality, the remaining grass in the central bay is assumed to have three major fates other than flowing out of the bay (broken line in Fig. 7): (1) washing ashore; (2) flowing back to the port areas and then being collected by the administrators; or (3) sinking to the seabed. Fate (1) would not be critical in the annual flow because the coastline of the bay is highly developed and most of the natural coast has disappeared (Furukawa and Okada, 2006). In addition, beached grass is eventually returned to the bay by tides and/or waves during one year because almost the entire natural coast is a tidal flat.

Ignoring fate (2) would result in overestimation of the inflow and outflow fluxes. However, we assume that the collected volume of grass flowing back to the port areas was relatively small because the time series of the daily volume collected by the port administrators (not shown) was significantly correlated with that of the river discharge of the three major rivers ($R = 0.73$, $P < 0.01$). This indicates that the port administrators have been collecting the grass directly after it flows into the bay from the rivers. Thus the overestimated volume by ignoring fate (2) would be relatively small.

At present, we do not have data for discussing the contribution of fate (3) (i.e. sinking process) to the annual flow. We assume that the portion of grass flowing in from rivers sinks because terrestrial vegetation has been found by a trawl survey on the seabed of the Southern California Bight (Moore and Allen, 2000). If grass is stored by sinking in the bay, it might contribute to the oceanic carbon cycle just like terrestrial dissolved and particulate organic carbon (Hedges et al., 1997). To determine the contribution of terrestrial natural debris to the marine ecosystem, we will estimate the flux of the natural debris sinking to the seabed in a future work.

Although the volume collected by the MLIT and the port administrators accounts for 39% of the annual inflow flux, we consider that they could perform clean-up operations more effectively. For example, grass was dense near the bay mouth on 3 June when the MLIT collected grass near the bay head (Fig. 6(b)). If information on patches of grass could be informed to the captain of the MLIT clean-up vessel, a larger amount of grass could be collected. Surface

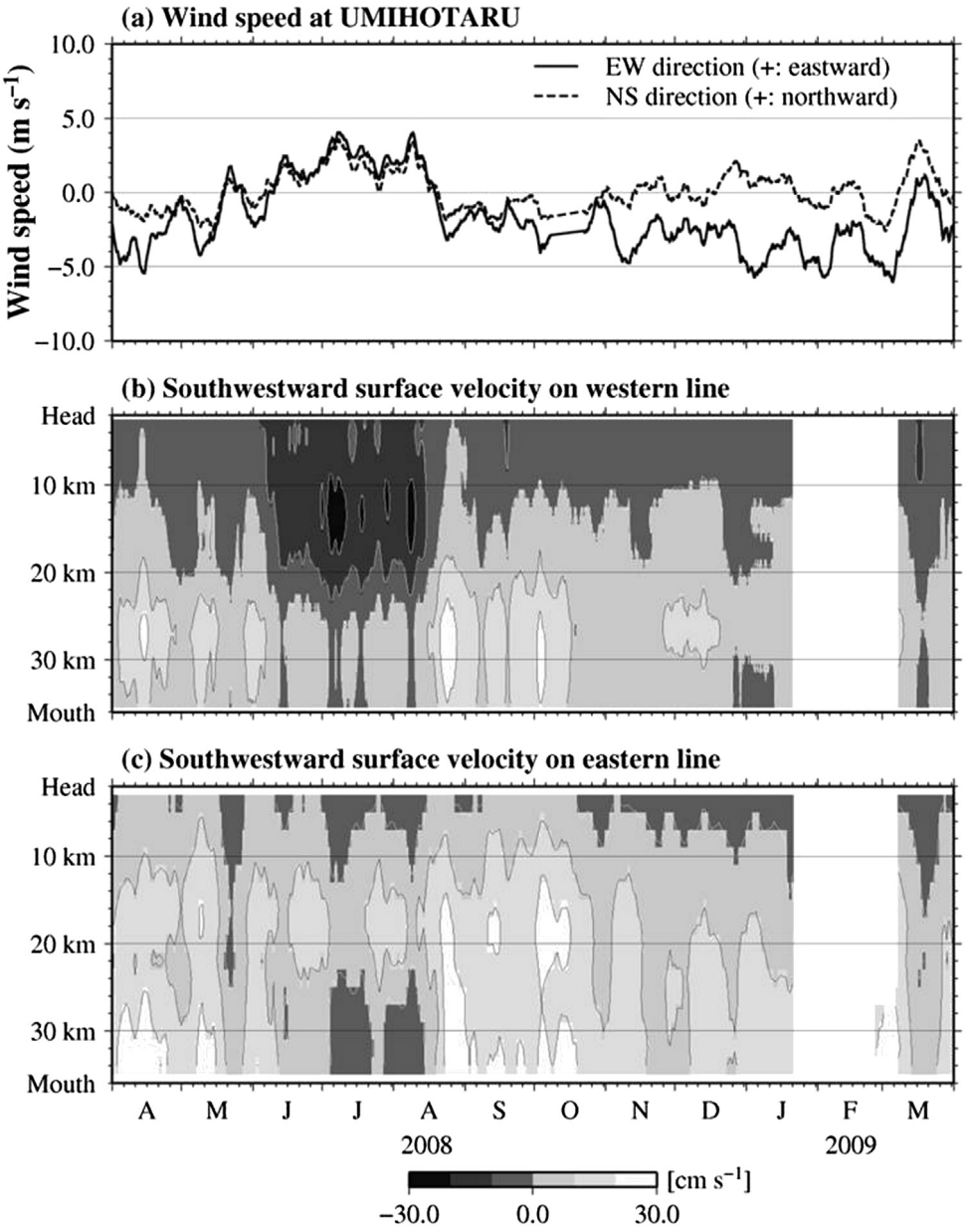


**Fig. 8.** (a) The time series of wind speed observed at *Umihotaru* by the Japan Coast Guard (diamond in Fig. 1(c)), (b) surface velocity measured by HF radar on the western line (solid thin line in Fig. 1(c)) and (c) eastern line (broken thin line in Fig. 1(c)). Wind speed and surface velocity are the 14-day moving averages. The top and bottom of the vertical axis of both (b) and (c) are the bay head and the bay mouth, respectively.

current velocities are available from HF radar systems in quasi-real time (Tokyo Bay Environmental Information Center; http://www.tbeic.go.jp/radar_tbeic/index.asp). River levels used to calculate the river discharge at the river mouth (see Section 2.4 or Nihei et al. (2007b)) are also measured by the MLIT in quasi-real time (Water Information System by the MLIT; http://www1.river.go.jp/). In the future, we will construct a prediction system by applying the PTM using quasi-real time surface current velocities and hourly inflow fluxes calculated by substituting the quasi-real time river discharge in Eq. (2) developed in this study.

In this study, to facilitate the particle-tracking experiments, we selected grass that has low windage (i.e. the ratio of the sail area of debris to its subsurface depth) as target natural debris (see Section 2.1). In the future, we will develop a PTM that takes the windage into account. The PTM with the windage effect would enable us to predict the movement of other natural debris with higher windage (e.g. wood and bamboo).

## 4. Discussion

### 4.1. Relationship between grass inflow flux and river discharge

Although the determination coefficient for the regression equation established by the IMLM was low because of the large variability of the LR for the SRD of 0.02–0.3 $m^3\ s^{-1}\ km^{-2}$, a significant relationship was found between the LR and the SRD (see Sections 3.1 and 3.2). The variability would be caused by: (1) a difference of the LR between the rising stage and the subsiding stage, (2) various cross sections of river channel in the catchment

area of rivers and (3) seasonal variations of the relationship between the LR and the SRD. We consider each of these in turn.

(1) The LRs obtained by the net sampling (Nihei et al., 2010) were classified into two groups (i.e. the LRs in the rising stage and those in the subsiding stage). The rising (subsiding) stage is defined when the SRD increases (decreases) during the net sampling. The net sampling data indicates that the LRs in the rising stage were one order of magnitude larger than those in the subsiding stage (Fig. 3). (2) The catchment area of the large rivers flowing into the bay is very large, and the river channels have been developed in the lower reaches (a typical cross-section is shown in the lower-right diagram of Fig. 3), and not developed in the upper reaches (i.e. a simple parabolic cross-section). The variability of the LR with the developed cross-section would temporally differ from that with a simple parabolic cross-section (Nihei et al., 2010). (3) The abundance of grass in the river channel would depend on the season; grass is more abundant in summer than in winter. These are important issues when estimating inflow fluxes of grass precisely. Thus the LR does not consistently increase in proportion to the river discharge.

At present, we do not obtain LRs for SRD values larger than 0.57 $m^3\ s^{-1}\ km^{-2}$ by the net sampling. It would be difficult to obtain LRs by the net sampling continuously because the personnel and cost required, especially during large flood events as the SRD is larger than 0.57 $m^3\ s^{-1}\ km^{-2}$. On the other hand, the IMLM can allow us to estimate LRs more easily than the net sampling because data collected systematically by the MLIT and HF radar-derived surface velocities are available. Thus, we can obtain LRs in large flood events and in every season on the SRD–LR diagram and improve the coefficient values (i.e. $a$ and $b$ in Eq. (2)) in the regression equation. In a future work, we will establish an inflow model that considers the seasonal variation (e.g. first flush) and the response to large flood events by obtaining the LRs through estimations by the IMLM in various years.

Long-term estimations of the LR will be useful for evaluating the effects of river development or clean-up along river banks and flood plains in the upper reaches. The LRs would gradually decrease as a result of taking such measures along river channels. And the IMLM enables us to conduct the long-term monitoring of the LRs.

### 4.2. Seasonal variation of residual volume

In the hindcast experiment, we found a seasonal variation of the monthly residual volume: it gradually increased from April to August 2008, and then greatly decreased in September 2008. The main cause of this variation would be a seasonal residual current in the bay. Fig. 8 shows the time series of the 14-day moving average surface velocity along the western line (solid thin line in Fig. 1(c)) and the eastern line (broken thin line in Fig. 1(c)) along the axis of Tokyo Bay. The southwestward current is positive in Fig. 8. The northeastward (southwestward) residual current along the western (eastern) line was generated in the range between 10 km and 20 km away from the bay head from the end of April to mid August (Fig. 8). This figure indicates that this current field consisted of an anti-cyclonic circulation near the bay head, and the northeastward (southwestward) residual current was strong (weak) in the period when a southwesterly wind was blowing (i.e. from June to mid August). A snapshot of the residual velocity field on 31 July is shown in Fig. 1(c) and indicates that the anti-cyclonic circulation is centered on the eastern side of the bay. On the other hand, the southwestward residual current was consistently generated when a northeasterly wind was blowing (i.e. from mid August to September).

The mechanism of generation of this residual current field is examined based on the balance between an anti-cyclonic circulation formed by the estuarine circulation (Fujiwara et al., 1997) and a wind-driven current (Hinata et al., 2010). According to Fujiwara et al. (1997), the anti-cyclonic circulation is generated in the upper layer near the bay head by the horizontal divergence associated with upward entrainment, which is part of the estuarine circulation.

The dependence of the wind-driven current was theoretically investigated using a linear steady-state analytical model based on Ekman solutions by Hinata et al. (2010). Their theory is applicable to Tokyo Bay because the bathymetry of the bay is approximated by a triangular cross-section as the basin axis shifts westward (Fig. 1(c)). The magnitude of the vertical diffusivity coefficient in Tokyo Bay is estimated to be $10^{-4}\ m^2\ s^{-1}$ (Guo and Yanagi, 1996). When estimating the Ekman number ($E$) using the diffusivity coefficient ($K = 10^{-4}\ m^2\ s^{-1}$), the Coriolis parameter ($f = 8.44 \times 10^{-5}\ s^{-1}$) corresponding to the latitude of 35.5° and the maximum water depth ($h = 20$ m) in the central bay, the magnitude is $10^{-2}$ (i.e. $E = K/fh^2 = 0.03$). With this magnitude of Ekman number, when the wind is blowing in the direction of the basin axis, the surface wind-driven currents in the shallower area (i.e. both coasts of the bay) and the deeper area (i.e. around the basin axis) are the strong current and the weak current for the downwind direction, respectively (see Fig. 10 in Hinata et al. (2010)).

Thus, the anti-cyclonic circulation was frequently generated by the estuarine circulation from the end of April to mid August. In particular, the northeastward (southwestward) current on the western (eastern) side became strong (weak) from June to mid August due to the wind-driven current formed by the southwesterly wind (i.e. wind toward the bay head along the bay axis), and its center shifted to the eastern side. On the other hand, the southwestward density-driven current intensified from mid August to September because of the large inflow flux of freshwater during a flood event (see Fig. 4(a)). During this event, the southwestward residual current prevailed consistently in the whole bay due to the northeasterly wind (i.e. wind toward the bay mouth along the bay axis).

Consequently, the monthly residual volume increased from April to August because grass was trapped in the bay due to the anti-cyclonic circulation. In particular, grass was easily trapped in the bay because the northeastward residual current of the circulation became strong due to the southwesterly wind blowing from June to mid August. The monthly residual volume greatly decreased in September because most of the grass immediately flowed out of the bay from mid August to September due to the southwestward residual current, which consisted of the density-driven current and the wind-driven current generated by the freshwater inflow and northeasterly wind, respectively.

## 5. Conclusions

We numerically estimated the inflow flux of terrestrial grass, which accounted for 29% of floating macro-debris collected by the Ministry of Land, Infrastructure, Transport and Tourism (MLIT), into Tokyo Bay from April 2008 to March 2009 (F2008) based on an “inverse method using a Lagrange multiplier” (IMLM) in conjunction with a two-way particle-tracking model (two-way PTM). In the numerical estimation, we used the high-frequency (HF) ocean surface radar-derived surface current velocities and the amount of grass collected by the MLIT using clean-up vessels.

The estimated hourly inflow flux was compared with the total river discharge of the three large rivers flowing into Tokyo Bay (Edo River, Ara River and Tama River). A significant relationship between the estimated loading rate (i.e. hourly inflow flux/total catchment area of the three large rivers (6571 $km^2$); LR) and the specific river discharge (i.e. river discharge/total catchment area; SRD) was found by regressing the LR against the SRD using Eq. (2) ($R^2 = 0.23$,

$P < 0.01$, see Fig. 3). The hourly inflow fluxes in certain periods that could not be estimated by the IMLM because either the MLIT clean-up vessels did not operate or the HF radar malfunctioned, were estimated using the regression equation between the LR and the SRD. Consequently, at least 2115 $m^3\ yr^{-1}$ of the grass flowed into the bay annually, and the contribution of flood events to the inflow flux of grass was larger than that of the inflow flux of freshwater. In the course of one year, 39% of grass flowing into Tokyo Bay was collected by the clean-up vessels in the bay, and 61% flowed out of the bay or sank to the seabed.

The low determination coefficient for the regression equation was due to the large variability of the LR for the SRD of 0.02–0.3 $m^3\ s^{-1}\ km^{-2}$ (Fig. 3). However, the large variability was reasonable because the LRs observed by the net sampling conducted by Nihei et al. (2010) were included within the 95% confidence interval of the regression residuals, and also largely varied in the same range of the SRD (Fig. 3). We consider that one of the reasons for the large variability is seasonal variation of the LR (see Section 4.1). At present, LRs in large flood events (i.e. SRD larger than 0.57 $m^3\ s^{-1}\ km^{-2}$) have not been obtained. The IMLM will be useful for establishing an inflow model that considers the seasonal variation (e.g. first flush) and the response to large flood events, because the LRs are systematically estimated by the IMLM using HF radar derived surface currents and data on debris collected by the MLIT (see Section 4.1).

To validate our estimation, we carried out a hindcast experiment and showed that the monthly net volume of grass actually collected by the MLIT was successfully reproduced by the experiment. This indicates that, in general, the hourly inflow fluxes of grass are successfully estimated in this study. In addition, we demonstrated the monthly residual volume in the bay and the monthly outflow from the bay mouth through the hindcast experiment, and found that the volume varied seasonally: it gradually increased from April to August 2008 and greatly decreased in September 2008. This seasonal variation depends on the surface residual current.

In the future, we will establish a prediction system to enable grass to be collected more effectively by the MLIT and the port administrators using HF radar-derived surface currents and the inflow model. In addition, we will estimate the sinking flux of natural debris to help understand the role of natural debris in marine ecosystems.

## Acknowledgments

The authors thank Dr. S. Kako of Kagoshima University, Dr. S. Kato of Toyohashi University of Technology and Dr. S. Aoki of Osaka University for their valuable comments, the Chiba Port Office of the Ministry of Land, Infrastructure, Transport and Tourism and the Port Administrators for providing the collected data on floating macro-debris, and Dr. A. Kuwae and Mr. E. Miyoshi for helping with the laboratory experiments. We also thank Dr. E. Wolanski, editor of this paper, and anonymous reviewers; their detailed and instructive comments improved this paper considerably. This research was supported by the Environment Research and Technology Development Fund (B-1007) of the Ministry of the Environment, Japan and by a Grant-in-Aid for Scientific Research (KAKENHI) (23656309, 25820234).

## Appendix A

The voids between pieces of grass are included in the volume of grass measured at the home port. Therefore, to estimate the net volume of grass, a “net ratio” (i.e., net volume/total volume including the void volume) was measured by a simple experiment in our laboratory. These experiments were conducted using approximately 30 L of sample grass that the MLIT collected in various seasons. In the experiment, 10 L of sample grass were placed in a 15-L cylinder, then the cylinder was filled with water. The volume of water that drained from the cylinder was measured using a beaker with a scale. The net volume was then obtained by subtracting the volume of drained water from the total volume. We conducted this experiment three times using the same sample grass, and determined the average net ratio as 0.3661.

## Appendix B

Before identifying the source and estimating the inflow flux, we conducted particle-tracking experiments to calculate the monthly residence time of the surface water masses; this time is used as the longest time duration for the backward-in-time PTM experiments. The particles were uniformly deployed at a spacing of 100 m in the area covered by HF radar at 00:00 every day and were carried by the HF radar-derived surface current. Specifically, the location $(x, y)$ of particle $\mathbf{X}$ at time $t + \Delta t$, where $\Delta t$ is the time increment (300 s), is given by

$$\mathbf{X}^{t+\Delta t} = \mathbf{X}^t + \mathbf{U}\Delta t + \frac{1}{2}\left(\mathbf{U}\cdot\nabla_{\mathrm{H}}\mathbf{U} + \frac{\partial \mathbf{U}}{\partial t}\right)\Delta t^2 + R\sqrt{2K_{\mathrm{h}}\Delta t}(\mathbf{i},\mathbf{j}), \tag{B.1}$$

where $\mathbf{U}$ $[=(u, v)]$ is the HF radar-derived surface current vector, $K_{\mathrm{h}}$ is the horizontal diffusivity which is modeled with the Smagorinsky formula for diffusion, $\mathbf{i}$ and $\mathbf{j}$ are unit vectors in the $x$ (east–west) and $y$ (north–south) directions, respectively, and $R$ is a random number generated at each time step with an average and standard deviation of 0.0 and 1.0.

We assumed that the particles reaching the bay mouth grid boxes (bold broken line in Fig. 1(c)) within each time step flowed out of the bay. If the particles reach other boundaries of HF radar coverage, they are returned to their location in the previous time step. This operation is repeatedly conducted until the particles return to offshore, and is referred to as “re-drifting operation”. The particle tracking was performed daily until 90% of the deployed particles flowed out, and the daily residence time was determined as the time until 90% of the particles flowed out. The maximum of the daily residence times in the month was used as the monthly residence time. The monthly residence time ranged from 19 to 60 days. The particles deployed from June to July showed the longest monthly residence time (60 days), and those deployed in September showed the shortest residence time (19 days).

## Appendix C

Nihei et al. (2010) conducted a net sampling at the Noda Bridge (black square in Fig. 1(b)) across the Edo River on 10–12 August 2009 and 8–9 October 2009. They collected debris on each river by suspending a 2.5-cm mesh net with a mouth measuring 1 m × 1 m for 1–5 min, and measured the fluxes of debris per unit width collected by the net. In the sampling, more than 94% of the collected debris was grass. The net sampling was conducted at only the center point on the lateral cross section of the river because of the difficulty of sampling at multiple positions on the bridge. To define a lateral distribution function of the flux per unit width on each observation, video images were taken simultaneously at multiple points on the bridges including the center point. The number of clearly identifiable debris pixels in sequential images was counted by eye. The fluxes per unit width were linearly correlated with the number of pixels at the same point. The unit-width fluxes at other points except the center point were calculated using the linear

correlation and the numbers of pixels at those points. The lateral distribution function was then determined by linearly interpolating the unit-width fluxes for the in-between points. The hourly inflow fluxes were calculated by integrating the function for the river width at the observation site (90 m).

## References


Armitage, N., Rooseboom, A., 2000. The removal of urban litter from stormwater conditions and streams: paper 1 – the quantities involved and catchment litter management options. Water SA 26, 181–188.

Durrum, E., 1997. The control of floating debris in an urban river. In: Coe, J.M., Rogers, D.B. (Eds.), Marine Debris, pp. 351–358.

Ebise, S., 1985. Storm runoff behaviours and loading of pollutants. J. Water Pollut. Res. 8, 499–504.

Fujiwara, T., Sanford, L.P., Nakatsuji, K., Sugiyama, Y., 1997. Anti-cyclonic circulation driven by the estuarine circulation in a gulf type ROFI. J. Mar. Syst. 12, 83–99.

Furukawa, K., Okada, T., 2006. Tokyo Bay: its environmental status—past, present, and future. In: Wolanski, E. (Ed.), The Environment in Asia Pacific Harbours. Springer, Netherlands, pp. 15–34.

Guo, X., Yanagi, T., 1996. Seasonal variation of residual current in Tokyo Bay, Japan—diagnostic numerical experiments. J. Oceanogr. 52, 597–616.

Hedges, J.I., Keil, R.G., Benner, R., 1997. What happens to terrestrial organic matter in the ocean? Org. Geochem. 27, 195–212.

Hinata, H., Kanatsu, N., Fujii, S., 2010. Dependence of wind-driven current on wind stress direction in a small semienclosed, homogeneous rotating basin. J. Phys. Oceanogr. 40, 1488–1500.

Isobe, A., Kako, S., Chang, P.-H., Matsuno, T., 2009. Two-way particle tracking model for specifying sources of drifting objects: application to the East China Sea Shelf. J. Atmos. Oceanic Technol. 26, 1672–1682.

Kako, S., Isobe, A., Seino, S., Kojima, A., 2010. Inverse estimation of drifting-object outflows using actual observation data. J. Oceanogr. 66, 291–297.

Kataoka, T., Hinata, H., 2012. Applicability of the inverse method for estimation of drifting-litter inflows to Tokyo Bay and its dependence on horizontal diffusivity. Bull. Coast. Oceanogr. 49 (2), 113–126 (in Japanese).

Law, K.L., Moret-Ferguson, S., Maximenko, N.A., Proskurowski, G., Peacock, E.E., Hafner, J., Reddy, C.M., 2010. Plastic accumulation in the North Atlantic subtropical gyre. Science 329, 1185–1188.

Moore, S.L., Allen, M.J., 2000. Distribution of anthropogenic and natural litter on the mainland shelf of the Southern California Bight. Mar. Pollut. Bull. 40, 83–88.

Moore, C.J., Moore, S.L., Leecaste, M.K., Weisberg, S.B., 2001. A comparison of plastic and plankton in the North Pacific central gyre. Mar. Pollut. Bull. 42, 1297–1300.

Nihei, Y., Ehara, K., Usuda, M., Itai, F., Shigeta, K., 2007a. Water quality and pollutant load in the Edo River, Ara River and Tama River. Proc. Coast. Eng. JSCE 54, 1226–1230 (in Japanese).

Nihei, Y., Takamura, T., Watanabe, N., 2007b. Issues on discharge monitoring in main influent rivers into Tokyo Bay. Proc. Coast. Eng. JSCE 54, 1221–1225 (in Japanese).

Nihei, Y., Shirakawa, A., Suzuki, T., Akamatsu, Y., 2010. Field measurements of floating-litter transport in a large river under flooding conditions and its relation to DO environments in an inner bay. J. JSCE, Ser. B2 (Coast. Eng.) 66, 1171–1175 (in Japanese).

Ryan, P.G., Moore, C.J., van Franeker, J.A., Moloney, C.L., 2009. Monitoring the abundance of plastic debris in the marine environment. Philos. Trans. Roy. Soc. B 364, 1999–2012.

Takada, H., Ogura, N., Ishiwatari, R., 1992. Seasonal variations and modes of riverine input of organic pollutants to the coastal zone: 1. Flux of detergent-derived pollutants to Tokyo Bay. Environ. Sci. Technol. 26, 2517–2523.

Yanagi, T., Shimizu, M., Nomura, M., Furukawa, K., 2003. Spring–neap tidal variations of residual flow in Tokyo Bay, Japan. Cont. Shelf Res. 23, 1087–1097.